Angle-azimuth decomposition of converted waves using extended images

Julio Oliva Frigerio, Colorado School of Mines and Petrobras

Paul C. Sava, Colorado School of Mines

Abstract

In this paper, we discuss an algorithm to decompose converted shear waves seismic data into angle gathers. This work is an extension to the work published by Sava and Vlad (2010), which presents an equivalent method for pure compressional waves. This method can be applied using a variety of solutions for the wave-equation and wave extrapolation, e.g. finite-difference, kirchhoff, and frequency-domain solutions. However, the power of this method is due to its applicability with finite-difference solution for the wave-equation and a consistent imaging condition. Hence, this method is able to deal with issues due to complex geology and fits perfectly the RTM migration.

Introduction

In regions characterized by complex subsurface structure, wave-equation depth migration is a powerful tool for accurately imaging the earths interior. The quality of the final image greatly depends on the quality of the velocity model and on the quality of the technique used for wavefield reconstruction in the subsurface (Gray et al., 2001). However, structural imaging is not the only objective of wave-equation imaging. It is often desirable to construct images depicting reflectivity as a function of reflection angles. Such images not only highlight the subsurface illumination patterns, but could potentially be used for image postprocessing for amplitude variation with angle analysis. Furthermore, angle domain images can be used for tomographic velocity updates. Decomposition of migrated images into angle and azimuth components is useful for several purposes, for example for illumination studies or AVAZ analysis. An algorithm for angle decomposition of pure acoustic waves using extended imaging condition has been recently presented by Sava and Vlad (2010). Here we show what changes have to be introduced in the algorithm so that the angle decomposition can be applied for converted waves. Our algorithm uses seismic wavefields reconstructed with the complete wave equation, thus it inherits all attributes of this methodology for imaging complex geologic structures. We use conventional modifications of wave-equation migration algorithms, for example by using different velocities for the the source and receiver wavefields, i.e. P-wave velocity for the source and S-wave velocity for the receiver wavefields. The angle decomposition is based on extended common image-point gathers. Such gathers are advantageous for wave-equation migration because they can be constructed at sparse locations in the image, thus reducing computational cost. Moreover, the common image point gathers are not biased toward the vertical direction, as is the case for conventional common-image-gathers, and they also avoid calculations in areas that are not useful for velocity analysis. These advantages are discussed in details by Sava and Vasconcelos (2011).

Extended Imaging Condition

The extended imaging condition differs from the conventional imaging condition in that it is a correlation between the source and receiver wavefields shifted in the space and in the time directions (Claerbout, 1971 and Sava and Vasconcelos, 2011).

$$R(\vec{x}, t, \vec{\lambda}, \tau) = \sum_t W_s(\vec{x} - \vec{\lambda}, t + \tau) W_r(\vec{x} + \vec{\lambda}, t - \tau) \qquad (1)$$

The equations defining the spatial extent of the incident and reflected wavefronts at a time t, considering the origin at (x_s, t_s) and (x_r, t_r), are:

$$\hat{n}_s \cdot (\vec{x} - \vec{x}_s) = v_s(t - t_s) \qquad (2)$$

$$\hat{n}_r \cdot (\vec{x} - \vec{x}_r) = v_r(t - t_r) \qquad (3)$$

The variables with index s are related to the source wavefield, and variables with index r are related to the receiver wavefield. If symmetrical space shifts ($-\lambda$ and $+\lambda$) are applied to each of these wavefronts, then a shift in time τ is necessary to bring them to a position where once again they cross the original point of reflection (Sava and Vlad, 2010). The relation between the spatial and temporal shifts are given by the equations

$$\hat{n}_s \cdot (\vec{x} - \vec{x}_s - \vec{\lambda}) = v_s(t - t_s - \tau) \qquad (4)$$

$$\hat{n}_r \cdot (\vec{x} - \vec{x}_r + \vec{\lambda}) = v_r(t - t_r + \tau) \qquad (5)$$

We can use equation 2 in equation 4 and equation 3 in equation 5 to cancel out the spatial and temporal variables, so that we end up with an expression which depends only with the lag variables:

$$\hat{n}_s \cdot \vec{\lambda} = v_s \tau \qquad (6)$$

$$\hat{n}_r \cdot \vec{\lambda} = v_r \tau \qquad (7)$$

The Moveout Equation

From equations 6 and 7 we want to extract one equation that defines a surface on the (λ, τ) domain. This surface must depend on v_s, v_r, the reflector's normal $\hat{n}$, the azimuth of reflection ϕ, and the angles of incidence θ_s and reflection θ_r. In order to find the dependence on $\hat{n}$, θ_s and ϕ, we have to understand the relation between these variables and n_s and n_r (figure 1):

$$\hat{n}_s = (\hat{n}_s \cdot \hat{q})\,\hat{q} + (\hat{n}_s \cdot \hat{n})\,\hat{n} \qquad (8)$$

$$\hat{n}_s = \sin\theta_s\,\hat{q} - \cos\theta_s\,\hat{n} \qquad (9)$$

$$\hat{n}_r = (\hat{n}_r \cdot \hat{q})\,\hat{q} + (\hat{n}_r \cdot \hat{n})\,\hat{n} \qquad (10)$$

$$\hat{n}_r = \sin\theta_r\,\hat{q} + \cos\theta_r\,\hat{n} \qquad (11)$$

Therefore, equations 6 and 7 become:

$$\sin\theta_s\,(\hat{q} \cdot \vec{\lambda}) - \cos\theta_s\,(\hat{n} \cdot \vec{\lambda}) = v_s\tau \qquad (12)$$

$$\sin\theta_r\,(\hat{q} \cdot \vec{\lambda}) + \cos\theta_r\,(\hat{n} \cdot \vec{\lambda}) = v_r\tau \qquad (13)$$

Substituting $(\hat{q} \cdot \vec{\lambda})$ from equation 12 in equation 13, we obtain

$$\sin(\theta_s + \theta_r)(\hat{n} \cdot \vec{\lambda}) = (v_r \sin\theta_s - v_s \sin\theta_r), \qquad (14)$$

therefore

$$\hat{n} \cdot \vec{\lambda} = \frac{(v_r \sin\theta_s - v_s \sin\theta_r)}{\sin(\theta_s + \theta_r)} = \frac{(v_r \sin\theta_s - v_s \sin\theta_r)}{\sin\theta_s \cos\theta_s + \sin\theta_r \cos\theta_r} \qquad (15)$$

Using Snell's law given by

$$\sin\theta_r = \frac{v_r}{v_s}\sin\theta_s \quad and \quad \cos\theta_r = \sqrt{1 - (\frac{v_r}{v_s}\sin\theta_s)} \qquad (16)$$

we reach the result

$$\hat{n} \cdot \vec{\lambda} = \frac{(v_r - v_s)}{\cos\theta_r + \frac{v_r}{v_s}\cos\theta_s} \qquad (17)$$

The only possible values for the angle of incidence are in the range between 0° and 90°. The angle of the reflected S-wave has to be smaller than 90° and bigger than 0°. In this case, the denominator of equation 17 is always bigger than zero, so that we can write:

$$\hat{n} \cdot \vec{\lambda} = 0 \qquad (18)$$

The result expressed by equation 18 is that only shifts parallel to the reflecting plane contribute in the extended imaging condition (equation 1). Now we can derive the moveout equation by replacing $(\hat{n} \cdot \vec{\lambda})$ in equation 13 from equation 12:

$$\sin(\theta_s + \theta_r)(\hat{q} \cdot \vec{\lambda}) = (v_r \cos\theta_s + v_s \cos\theta_r)\,\tau \qquad (19)$$

Using the definitions

$$\theta \equiv \frac{\theta_s + \theta_r}{2} \quad and \quad \theta \equiv \frac{\theta_s - \theta_r}{2} \qquad (20)$$

in the moveout equation 19, we obtain the moveout equation in terms of θ and δ:

$$\sin(2\theta)\,(\hat{q} \cdot \vec{\lambda}) = [(v_r \cos(\theta + \delta) + v_s \cos(\theta - \delta)]\,\tau \qquad (21)$$

Quantities δ and θ are related by Snell's law:

$$\tan\delta = \tan\theta \left[\frac{1 - \gamma}{1 + \gamma}\right] \quad \gamma \equiv \frac{v_r}{v_s} \qquad (22)$$

Instead of θ and δ, we can also derive the moveout equation for θ_s and θ_r separately. From equation 19 we have:

$$(\sin\theta_s\,\cos\theta_r + \sin\theta_r\,\cos\theta_s)\,(\hat{q} \cdot \vec{\lambda}) = (v_r \cos\theta_s + v_s \cos\theta_r)\,\tau \qquad (23)$$

Considering equation 16 and defining the coefficients

$$\beta_s \equiv \frac{v_r}{v_s} + \frac{\sqrt{1 - \left(\frac{v_r}{v_s}\sin\theta_s\right)}}{\cos\theta_s} \qquad (24)$$

$$\beta_r \equiv \frac{v_s}{v_r} + \frac{\sqrt{1 - \left(\frac{v_s}{v_r}\sin\theta_r\right)}}{\cos\theta_r} \qquad (25)$$

we obtain the moveout equations for θ_s and θ_r

$$\beta_s\,\sin\theta_s\,(\hat{q} \cdot \vec{\lambda}) = \beta_s v_s\tau \qquad (26)$$

$$\beta_r\,\sin\theta_r\,(\hat{q} \cdot \vec{\lambda}) = \beta_r v_r\tau \qquad (27)$$

Cancelling out β_s and β_r on both sides we get moveout equation with the same form of that for PP waves presented by Sava and Vlad (2010):

$$\sin\theta_s\,(\hat{q} \cdot \vec{\lambda}) = v_s\tau \qquad (28)$$

$$\sin\theta_r\,(\hat{q} \cdot \vec{\lambda}) = v_r\tau \qquad (29)$$

Angle-azimuth decomposition for converted waves

The algorithm for decomposing converted waves into azimuth and angle of reflection is similar to that of acoustic waves presented by Sava and Vlad, 2010. The only differences are that, instead of one, two velocities must be used in the computation, vs and vr , and also the decomposition can be done in relation to three types of angle: θ, θ_s , or θ_r.

Synthetic example

We test the algorithm with a simple synthetic model. The model has homogenous velocity with the shear velocity being half of the acoustic velocity. The density is a step function, so that there is one single horizontal reflector in the model at the depth 1.0. Note that no spatial units are needed here, since we are dealing with angles, only relative coordinates matter.

This modeling considers a source of P-waves located at a point with coordinates Sx = 4.0, Sy = 4.0, Sz = 0.0. The isotropic elastic wave equation is used to propagate the waves generated by the source through a finite-difference algorithm. The results below show an analysis

```
CIP loop                       c = 1 ... N{
read reflector dip             n̂
read azimuth reference         v
rotate azimuth reference       {n̂, v} ⟶ a
read velocities                v_s and v_r
read CIP                       R(λ, τ)
azimuth angle loop             loop φ = 0° ... 360°{
rotate by azimuth                   {n̂, φ, a} ⟶ q̂
reflection angle loop               loop θ = 0° ... 90°{
apply slant stack              (equation 22)    R(λ, τ) ⟹ R(φ, θ)
                               (equation 28) or R(λ, τ) ⟹ R(φ, θ_s)
                               (equation 29) or R(λ, τ) ⟹ R(φ, θ_r)
                                    }
                               }
write                          R(φ, θ)
                               }
```
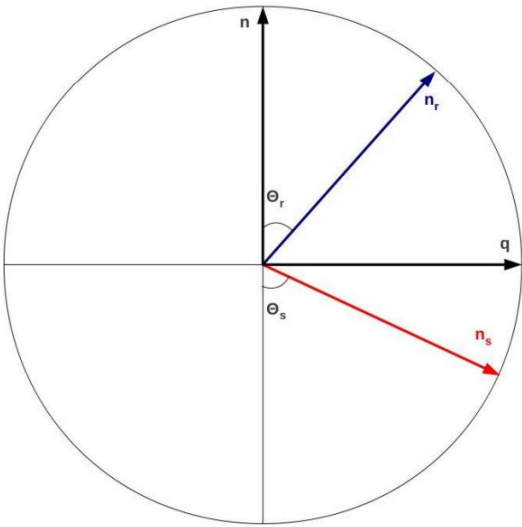

Figure 1: Geometry used in the derivation of the move-out function. The unit vector $\hat{n}$ defines the reflecting plane and is orthogonal to it. The unit vector $\hat{q}$ is parallel to the reflecting plane and defines the azimuth of reflection. The unit vectors $\hat{n}_s$ and $\hat{n}_r$ are orthogonal to the wave fronts of the source and receiver wavefields, respectively.

of the reflections at the CIP (common image point) with coordinates CIPx = 3.2, CIPy = 3.2, CIPz = 1.0 (Figures 2 and 3). Note that although here we have used here the isotropic elastic wave equation, any approximation of the wave equation is suitable for this algorithm.

The incident wave gives rise to two reflected waves, an acoustic and a shear waves. As the reflector is a horizontal surface, both waves must propagate in the same azimuthal direction. However, the angle of reflection of the acoustic wave is bigger than that of the shear waves. Figures 4 and 5 show the the images (migrated sections in space domain) for the PP and the PS experiments. Notice that the image obtained from PS waves presents polarity reversal.

Figures 6 and 7 illustrate CIP gathers for PP and PS reflections. The decomposition of the CIP gather in angles of reflection results in the angle-azimuth maps shown by Figures 8 and 9. Figures 8 and 9 show the azimuth of the reflection and the average between incidence and reflection angles for the PP and PS cases, respectively.

The azimuth of a point in these maps is represented by the azimuth of the line connecting this point to the center of the map. The average angle is represented by the distance from this point to the center of the map. The region between two consecutive circles spams a range of 15°. Note that both PP and PS reflections occur at the same azimuth, but the PS wave has smaller angle of reflection.

Analytical computations predict $\theta_{ps} = 22.0^o$ and $\theta_{pp} = 48.5^o$, where θ_{ps} and θ_{pp} are the average between incidence and reflection angles for PP and PS cases. The results observed in Figures 8 and 9 are in accordance with this prediction. On the angle-azimuth maps events associated with PP and PS reflections are fuzzy due to the bandlimited character of the waves propagated in this synthetic experiment. The predicted angles fall in the fuzzy region of each corresponding event.
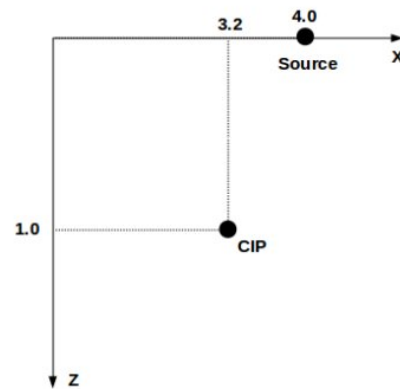

Figure 2: Vertical cross-section showing locations of the source point and of the CIP. Units are not provided since we are dealing with relative coordinates.
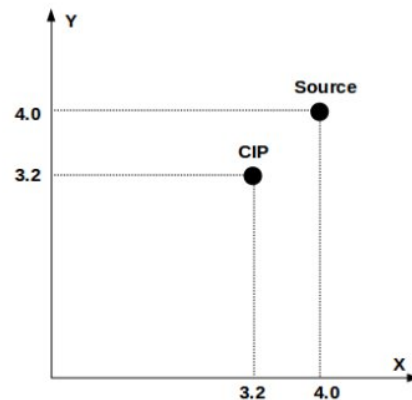

Figure 3: Map showing locations of the source point and of the CIP. Units are not provided since we are dealing with relative coordinates.

Conclusions

We present an algorithm for decomposing CIPs obtained by wave-equation migration of converted waves into reflection and azimuth angles. The method is similar to that of purely acoustic waves. In the PS algorithm, the moveout
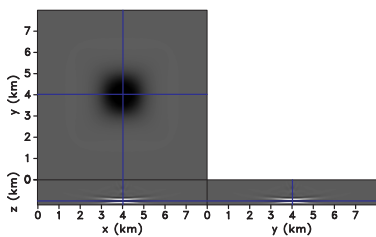
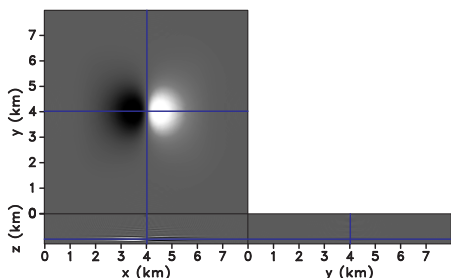Figure 4: Image in the space-domain constructed from PP-waves.

Figure 5: Image in the space-domain constructed from PS-waves.

equation distinguishes between the velocity of source wavefield and the velocity of the receiver wavefield. This algorithm is suitable to any method of wave propagation, the only requirement is that the source and receiver wavefields must be known at all times, which is common for reverse-time migration algorithms. The algorithm is robust and efficient and potentially allows for illumination studies and AVA analysis of converted waves.

References

Claerbout J.F., 1985, Imaging the Earth's Interior, Blackwell Scientific.

Gray, S. H., J. Etgen, J. Dellinger, and D. Whitmore, 2001, Seismic migration problems and solutions: Geophysics, 66, 16221640.

Sava, P.C., Vlad, I., 2011, Wide-azimuth angle gathers for wave-equation migration, Geophysics, in press.

Sava, P.C.,Vasconcelos, I., 2011, Extended imaging condition for wave-equation migration, Geophysical Prospecting, v. 59, no. 1, pp. 35-55.
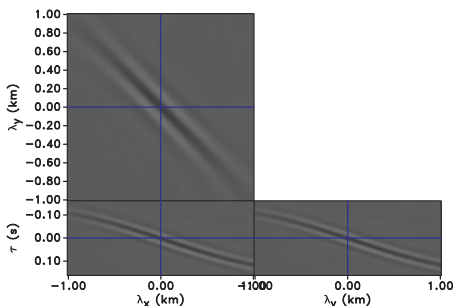
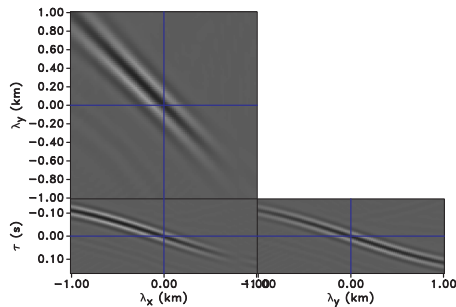Figure 6: CIP gathers for PP-waves.
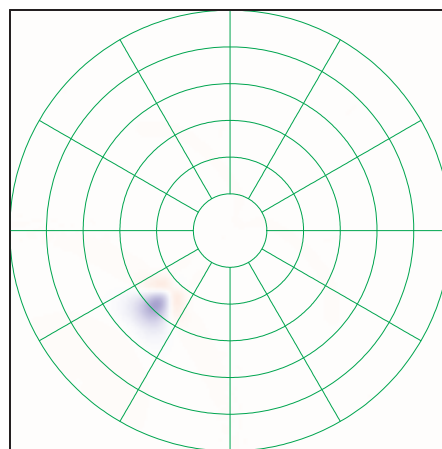

Figure 7: CIP gathers for PS-waves.

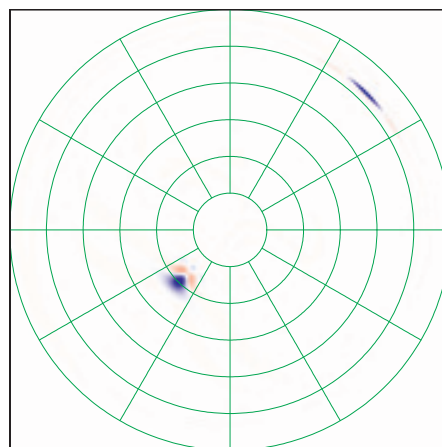Figure 8: Angle-azimuth diagrams of the CIPs for PP-waves.

Figure 9: Angle-azimuth diagrams of the CIPs for PS-waves. An artifact is present on the top right of the diagram.